Spectrochimica Acta Part B: Atomic Spectroscopy 214 (2024) 106899

Contents lists available at ScienceDirect

Spectrochimica Acta Part B: Atomic Spectroscopy

journal homepage: www.elsevier.com/locate/sab

In situ chemical analysis of duplex stainless steel weld by laser induced breakdown spectroscopy☆

Lukas Quackatz [a,*,1], Igor Gornushkin [a,2], Axel Griesche [a,1], Thomas Kannengiesser [a,b,1,3], Kai Treutler [c,4], Volker Wesling [c,4]

[a] Federal Institute for Materials Research and Testing (BAM), Unter den Eichen 87, 12205 Berlin, Germany
[b] Otto-von-Guericke University Magdeburg, Faculty of Mechanical Engineering, Institute of Materials and Joining Technology, Universitätsplatz 2, 39106 Magdeburg, Germany
[c] Institute for Welding and Machining, TU Clausthal, 38678 Clausthal-Zellerfeld, Germany

ARTICLE INFO

Keywords:
Duplex stainless steels
In situ measurement
LIBS
GMAW

ABSTRACT

The high corrosion resistance and good mechanical properties of duplex stainless steel (DSS) are due to its special chemical composition, which is a balanced phase ratio of ferrite (α) and austenite (γ). Many industrial applications require the integration of DSS components. For this, Gas tungsten arc welding (GTAW) is an excellent choice, as it allows an automated operation with high reproducibility. However, when the weld pool solidifies, critical ratios of α- and γ- phases can occur, which lead to solidification cracking, increased susceptibility to corrosion, and a decrease in ductility and critical strength. Previous studies have shown that these defects can be caused by the accumulation of manganese and chromium in the heat affected zone (HAZ), requiring ongoing monitoring of this accumulation. A suitable method for such monitoring is laser-induced breakdown spectroscopy (LIBS), which can be used in two operating modes: calibration using standard reference samples and calibration-free. Unlike conventional quantitative LIBS measurements, which require reference samples to generate a calibration curve, calibration-free LIBS (CF-LIBS) allows chemical compositions to be determined solely from the emission spectrum of the plasma. Numerous publications show that CF-LIBS is a fast and efficient analytical method for the quantitative analysis of metal samples. In this work, CF-LIBS is applied to spectra obtained during GTAW DSS welding and the result is compared with those obtained by PLS analysis. A good correlation was found between both types of analysis, demonstrating the suitability of the CF-LIBS method for this application. The CF-LIBS method has a significant advantage over conventional LIBS due to the rapid in situ measurement of concentrations of major alloying elements without calibration procedure. This, combined with fast feedback and appropriate adjustment of welding parameters, helps prevent welding defects.

1. Introduction

Duplex stainless steels (DSS) have excellent corrosion behavior and good mechanical properties, which is why they find various applications in industry where this combination is required. Examples include maritime structures, power plant components and chemical equipment. The microstructure of DSS consists of a balanced ratio between austenite (γ) and ferrite (α), which enables the outstanding properties of these steels [1,2]. For many industrial applications, DSS must be welded. Arc welding processes are a common method. Due to the complex process sequence and the large number of influencing factors, the latter must be precisely controlled. Welding processes are challenging, especially for

☆ This work was presented at the EMSLIBS 2023 conference in Porto, Portugal. https://opus4.kobv.de/opus4-bam/frontdoor/index/index/docId/58314

* Corresponding author.
E-mail addresses: lukas.quackatz@bam.de (L. Quackatz), Igor.gornushkin@bam.de (I. Gornushkin), Axel.griesche@bam.de (A. Griesche), Thomas.kannengiesser@bam.de (T. Kannengiesser), office@isaf.tu-clausthal.de (K. Treutler), office@isaf.tu-clausthal.de (V. Wesling).
[1] Federal Institute for Materials Research and Testing, 9.4 Weld mechanics, Unter den Eichen 87, 12,205 Berlin.
[2] Federal Institute for Materials Research and Testing, Unter den Eichen 87, 12,205 Berlin.
[3] Otto-von-Guericke University Magdeburg, Faculty of Mechanical Engineering, Institute of Materials and Joining Technology, Universitätsplatz 2, 39,106 Magdeburg, Germany.
[4] Institute for Welding and Machining, TU Clausthal, 38,678 Clausthal-Zellerfeld, Germany.

https://doi.org/10.1016/j.sab.2024.106899
Received 9 October 2023; Received in revised form 26 January 2024; Accepted 13 March 2024
Available online 21 March 2024

duplex steels, where ideal mechanical properties as well as corrosion resistance are achieved through precise temperature control and optimal chemical composition [3,4]. A minimum ferrite content is required in the weld metal (WM), as well as in the heat-affected zone (HAZ) [5,6]. An unbalanced γ/α phase ratio of 80–90% vol.-% α in WM leads to significant cracking problems in safety-critical components [7]. To prevent ferritization of the WM and to counteract the burn-off of alloying elements during welding, high-alloy filler metals are used. They promote the precipitation of γ through an increased concentration of γ-formers. The influence of these filler metals on the mechanical properties and microstructure of stainless steels can be found in [8,9]. Welding-induced burn-off of alloying elements, for example Mn or Ni, can significantly influence the phase formation of γ. This has a high impact for the resulting mechanical properties and corrosion resistance of the weld seam and thus the integrity of the resulting welded component. The aforementioned challenges in DSS welding highlight the need for an in situ measurement method to quantitatively and rapidly measure chemical concentrations during welding to prevent evaporation of alloying elements and measure minimal changes in the process.

Laser-induced breakdown spectroscopy (LIBS) provides highly accurate, virtually non-destructive quantitative measurements of chemical compositions. The measurements are possible both time and spatially resolved during welding, i.e., before, during and after solidification of WM and HAZ. LIBS is a spectroscopic method based on the element-specific photon emissions of the plasma [10]. To be able to perform quantitative analysis, the measurement method must be calibrated. There is currently no standardized calibration procedure; various regression algorithms are used, differing in complexity and computational costs. For example, multivariate calibration using partial least squares (PLS) is widely used. The relationship between the studied integral line intensity of the element and the known concentration based on various certified reference samples (calibration samples) is determined [11]. This calibration model can then be applied to similar (identical matrix) samples containing unknown element concentrations. The PLS method is reliable and not susceptible to spectral interferences [12]. However, multiple reference samples are needed for accurate calibration, and if matrix-matched standards are not available, matrix effects can make it difficult to predict unknown chemical concentrations. To overcome these drawbacks, the calibration-free method (CF) can be used for quantification. This method is already used in industrial environments, as well as in applications where reference samples are not available, such as working with cultural artifacts or biological samples [13–15]. The commonly used CF-LIBS is based on the Boltzmann plot method, which requires stoichiometric ablation and homogeneous isothermal optically thin plasma under local thermodynamic equilibrium (LTE) conditions [16–18].

A common welding process is gas tungsten arc welding (GTAW), in which an arc is created between a tungsten electrode and the workpiece using a sufficiently high current. Shielding gas is used to prevent oxidation of the workpiece and electrode [19]. The high heat flux of the welding plasma melts the workpiece and forms a melt pool. By using suitable welding parameters (e.g., adjustable welding current), the resulting microstructure can be controlled [20]. As the molten material evaporates, metal vapors can be released from the surface of the weld pool and condense again in cold areas. This loss of material can affect the microstructure of the weld and lead to deterioration of material properties [21]. The main mechanisms of evaporation of alloying elements during welding are explained in [22,23].

The combination of LIBS and welding has already been implemented by several research groups. Mirapeix et al. [24] developed a LIBS measurement setup to detect welding defects during a GTAW welding process. They investigated changes in welding current leading to surface defects and were able to qualitatively characterize the defects using LIBS. They also confirmed their results offline using LIBS 2D scanning of welds [25]. Lednev et al. [26–28] were also able to distinguish defect-free welds from defective ones by performing LIBS elemental analysis in the melt pool during the welding process.

Our previous work [29–33] has validated the in situ LIBS method for measuring chemical concentrations in GTAW of stainless steels. In this work, chemical concentrations are quantified during welding using PLS calibration. To further simplify and speed up chemical analysis, for the first time, we used the CF-LIBS procedure to quantitatively measure DSS chemical concentrations during GTAW welding. The results of the two methods are compared and the reliability of CF-LIBS is confirmed. The weld microstructure of DSS is controlled using filler metals. In this publication, filler metals are coated with either ferrite or austenite stabilizing elements to change the volume fraction of the respective phases. This has a significant influence on the mechanical properties of the welded component. We present a possibility to measure the chemical concentrations without prior calibration of the measuring system, in situ during welding to control weld defects and the resulting microstructure.

2. Experimental

2.1. Samples

Tests were carried out using standard duplex steel EN 1.4462 as the base material. The filler metal had a diameter of 1.6 mm and was supplied by Merkle Schweißtechnik Berlin GmbH. Chemical concentrations were determined by spark emission spectroscopy (OES) and are listed in Table 1. Material DSS EN 1.4462 served as the base material for the study, and material EN 1.4550 served as the filler metal for GTAW welding [34]. (See Fig. 1.)

For in situ LIBS tests, flat specimens measuring 150 × 35 × 5 mm^3 (length × width × thickness) were prepared. Before welding tests, the samples were cleaned with acetone to remove impurities that arose during production and processing.

In the approach presented here, welding electrodes are modified using a physical vapor deposition (PVD) system so that their chemical composition is different from the base material. Magnetron sputtering is used as a special variant of the coating process. With this process, various elements can be applied to the base material in thin film layers. In this publication, the elements Nb, Cu, Si, Ni and Mn were selected because they are the main alloying elements of DSS or have a very large influence on the resulting microstructure of the weld metal. The thickness of the thin film layer created on the substrate correlates with the coating time and is therefore controllable. After the welding wire has been fed, the application of high voltage in the evacuated process chamber causes the shielding gas to ionize. Positively charged gas ions are accelerated and collide with the cathode (target). Due to the transfer of momentum, atoms and molecules are released from the coating material. The material evaporated in this way condenses on the entire accessible surface and therefore also on the welding filler metal. This process is described in detail in [35,36].

2.2. Experimental setup

The welding tests were carried out using the CastoTIG 1611 DC GTAW welder from Castolin. A pure tungsten electrode with a diameter of 1.6 mm was used. All welding experiments were carried out at a shielding gas flow rate of 10 l/min with argon (Ar). The electrode was located at 2 mm from the part, and the diameter of the gas nozzle was 6 mm. Using a linear motor, the samples were welded at a constant speed of 10 cm/min. A narrow filler metal (Ø = 1.6 mm) with a coating was fixed in the center of the sample by spot welding. This made it possible to ensure continuous admixture of the filler metal to the base metal during the welding process. The LIBS system consists of a pulsed Nd:YAG laser with a wavelength of 1064 nm, a repetition rate of 15 Hz, and a maximum pulse energy of 200 mJ. The laser head is tilted 20° with respect to the surface normal to focus the laser spot precisely on the surface of the sample at a distance of 10 mm from the weld bead. A lens

Table 1
Chemical compositions of the materials used, measured with OES.

Material (EN 10088)	Chemical composition (wt.-%)										
	C	Si	Mn	P	S	N	Cr	Ni	Mo	Cu	Nb
1.4462	0.02	0.32	1.68	0.03	0.002	0.19	22.65	5.79	2.97	0.06	0.03
1.4550	0.05	1.79	1.12	0.02	0.003	0.02	18.70	9.71	0.06	0.07	0.62

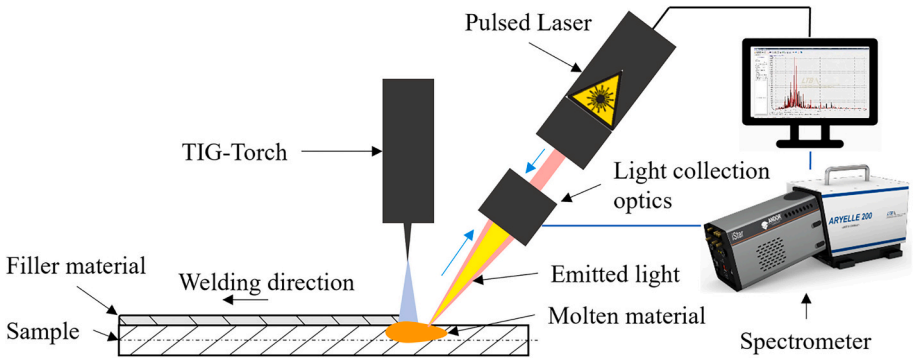

Fig. 1. Schematic sketch of the test setup. The filler material in the form of a wire was fixed in the center of the sample and moved under computer control using a linear table.

with a focal length of 300 mm was used to focus the laser beam on the sample surface. Element-specific light was detected and analyzed using an echelle spectrometer (Aryelle 200, LTB Berlin) equipped with an ICCD camera (Andor). The spectrometer/detector assembly was intensity calibrated over the spectral range 200–850 nm using a standard light source (Avantes). Plasma radiation was collected by a lens with a focal length of 10 mm connected to an optical fiber and directed to a spectrometer. All experiments used a gate width of 40 μs and a delay time of 1 μs. The surface temperature of the samples was measured during the melting process using an infrared pyrometer. The laser spot diameter was 100 μm and the energy per pulse was 200 mJ.

2.3. Data processing

The partial least squares (PLS) method was used to analyze the major alloying elements in the DSS and the deposited elements in the filler metal during welding. For this purpose, certified reference materials of the BAM Federal Institute for Materials Research and Testing (Germany) were used. It has been shown that the PLS method is well suited for the welding process since it is insensitive to external influences [37,38]. The PLS calibration model has already been validated in previous publications against other traditional chemical analysis methods [32].

In CF-LIBS, the integrated line intensities of the elements were used to generate individual Saha-Boltzmann plots. The plasma electron density was estimated from the width of lines with known Stark broadening parameters; the exact procedure can be found in [39]. Element lines for CF-LIBS and PLS analysis were selected based on the criteria of high intensity, minimal spectral interference, and low self-absorption. The latter means that mostly non-resonant lines with a low to medium transition probability are used. The list of lines for analysis of Fe-based samples is given in Table 2.

Fig. 2 shows a spectrum of a duplex steel EN 1.4462. The measurement was carried out at room temperature. The elements Mn and Fe are labeled.

3. Results and discussion

3.1. Weld microstructure

Following the welding tests, transverse sections of the specimens were made, and the microstructure was evaluated. The γ/α ratio was determined by image analysis. This allowed the influence of the coated welding consumables on the microstructure to be investigated. For this purpose, the specimens were etched with Beraha II color etch and imaged at different locations using an optical microscope. Overview images, detailed images of the base metal and the weld metal were taken. Fig. 3 (a) shows an overview of the weld microstructure of specimen Nb 6 h (coating element and coating duration for the filler metal). The specimen was welded at 160 A and 10 cm/min. Detailed micrographs of specimen Nb 6 h and Cu 6 h can be seen in Fig. 3 (b) and 3 (c), respectively. The microstructure has the usual appearance of a DSS weld microstructure. The base metal has a balanced phase ratio. In the weld metal, austenite precipitates at the grain boundaries, resulting in a Widmanstätten microstructure. This microstructure is especially pronounced in Fig. 3 (c). Image analysis was used to measure the volumetric austenite content. Table 3 shows the volumetric ferrite content of all samples. It can be seen that for austenite-stabilizing elements, such as Ni, Mn and Cu, the volume fraction of ferrite is reduced compared to

Table 2
Lines for CF-LIBS and PLS Analysis of iron-based samples.

Element	Ionic state	Emission lines
Iron	Fe I	295.69 nm, 306.72 nm, 356.90 nm, 358.119 nm, 368.76 nm, 370.95 nm, 372.78 nm, 374.36 nm, 374.95 nm, 375.82 nm, 376.72 nm, 404.58 nm, 442.73 nm, 448.22 nm, 452.86 nm, 491.90 nm, 492.05 nm
Iron	Fe II	258.59 nm, 259.15 nm, 259.28 nm, 271.44 nm
Manganese	Mn I	279.48 nm, 279.83 nm, 280.11 nm, 369.65 nm, 403.08 nm, 403.31 nm, 403.45 nm, 406.35 nm
Manganese	Mn II	257.61 nm, 260.57 nm, 293.31 nm, 293.93 nm, 344.20 nm, 348.29 nm
Chromium	Cr I	434.45 nm, 435.18 nm, 520.45 nm, 520.60 nm, 520.84 nm
Chromium	Cr II	266.60 nm, 266.87 nm, 267.18 nm, 284.32 nm, 284.98 nm, 311.87 nm, 312.04 nm
Nickel	Ni I	299.45 nm, 301.20 nm, 319.71 nm, 336.96 nm, 356.64 nm
Nickel	Ni II	241.61 nm
Silicon	Si I	251.61 nm
Copper	Cu I	324.75 nm, 327.40 nm
Molybdenum	Mo I	317.03 nm, 319.40 nm, 386.41 nm

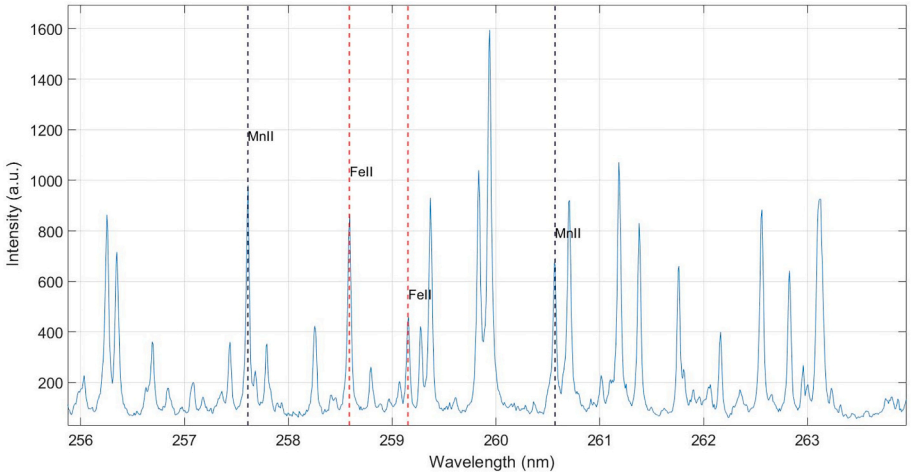

Fig. 2. LIBS spectrum of a EN 1.4462 with labeled element lines Mn and Fe.

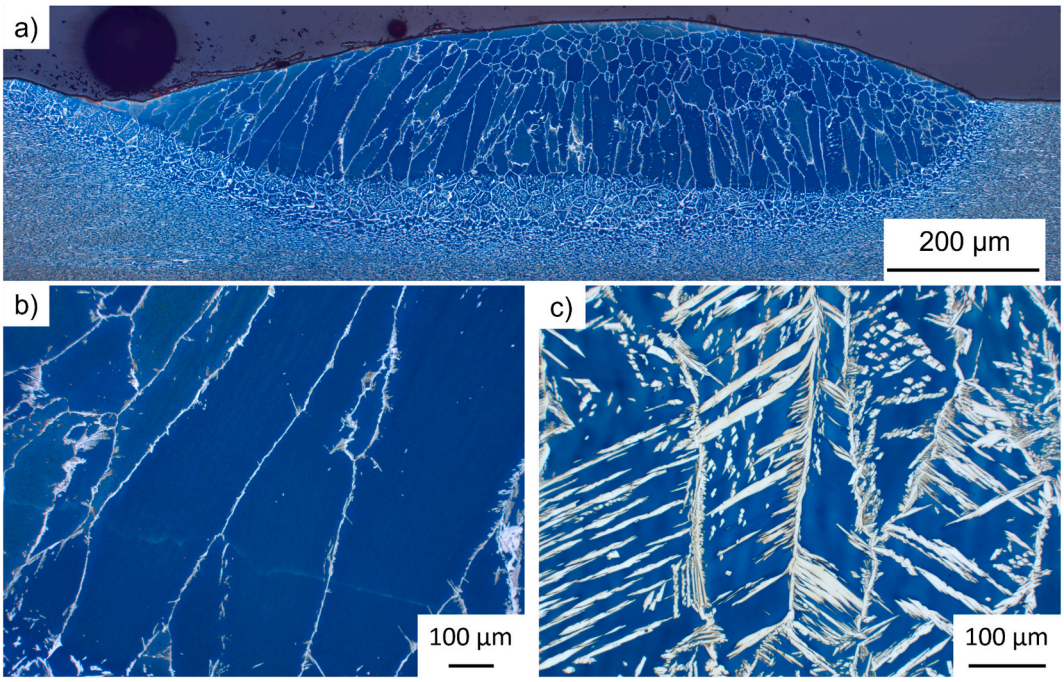

Fig. 3. Images of the weld microstructure 160 A, 10 cm/min. Bright: austenite, dark: ferrite; (b) overview image of the entire weld of sample Nb 6 h; (b) detail image of the weld microstructure of sample Nb 6 h, with 94 vol-% ferrite; (c) detail image of the weld microstructure of sample Cu 6 h, with 76 vol-% ferrite.

Table 3
Ferrite volume fraction of all examined weld specimens with associated coating element and duration.

Element + coating duration	Ferrite fraction
Nb 6 h	94 vol.-%
Nb 2 h	90 vol.-%
Cu 6 h	76 vol.-%
Cu 2 h	83 vol.-%
Mn 30 h	78 vol.-%
Mn 10 h	74 vol.-%
Ni 6 h	75 vol.-%
Ni 2 h	78 vol.-%
Si 6 h	80 vol.-%
Si 2 h	79 vol.-%

ferrite-stabilizing elements (Nb, Si). This proves that the coating of welding consumables with individual elements has a strong influence on the resulting microstructure of the weld metal. This change in the volumetric content of ferrite and especially the low volumetric content of austenite, for example, in the Nb 6 h sample, leads to a deterioration in the physical properties of duplex steels. For example, corrosion resistance is significantly reduced, and mechanical properties are deteriorated. Regulations [5] require that the ferrite volume content be maintained at a level of 30–70%.

3.2. *In situ measurements*

In situ LIBS measurements were performed during welding followed by PLS and CF-LIBS data processing. Preliminary tests were carried out on the base metal. Fig. 4 shows a series of Saha-Boltzmann plots (SBP) for all elements of the sample except Nb. The main element used to create SBP is Fe as it is the most abundant element in the sample. All

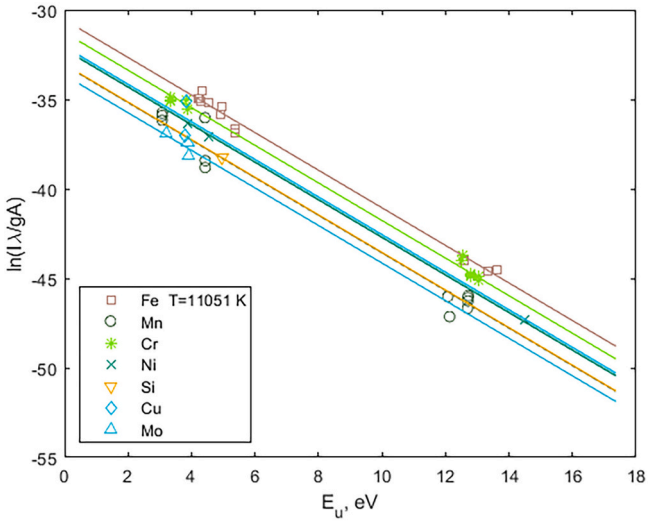

Fig. 4. Saha-Boltzmann plots (SBP) for all elements except Nb, measured in the base metal without welding.

other graphs are parallel to the main SBP. The procedure for creating an SBP involves correcting all lines for self-absorption. This procedure is described in detail in [17,39]. Self-absorption occurs when the emitted light is absorbed by the plasma before it reaches the detector. This can lead to distortions in the measured spectra and affect the accuracy of the analysis. To correct for self-absorption, the width and integrated intensity of a line is measured. Then the line width is estimated for hypothetical optically thin conditions using the algorithm proposed in [17] and, finally, the corrected integrated line intensity is determined based on the pre-calculated theoretical dependence of the thin/thick line width ratio on the thin/thick integral intensity ratio. It is important to note that the self-absorption degree depends on several factors, including the experimental conditions, the properties of the sample matrix and the analytical methods used.

As an example, for the Ni 6 h sample, the change in chemical concentrations during the welding process is shown in Fig. 5 (a). The welding process begins with spectrum No. 5 and ends with spectrum No. 25. After this, the sample is only cooled, without welding. It is noteworthy that during the welding process, according to CF-LIBS data, the Mn concentration increases. This was already observed in [33] and may be due to the low enthalpy of vaporization of Mn (220 kJ/mol). Mn can evaporate during welding, so it is measured by LIBS not only on the surface of the sample, but also in the atmosphere near the welding

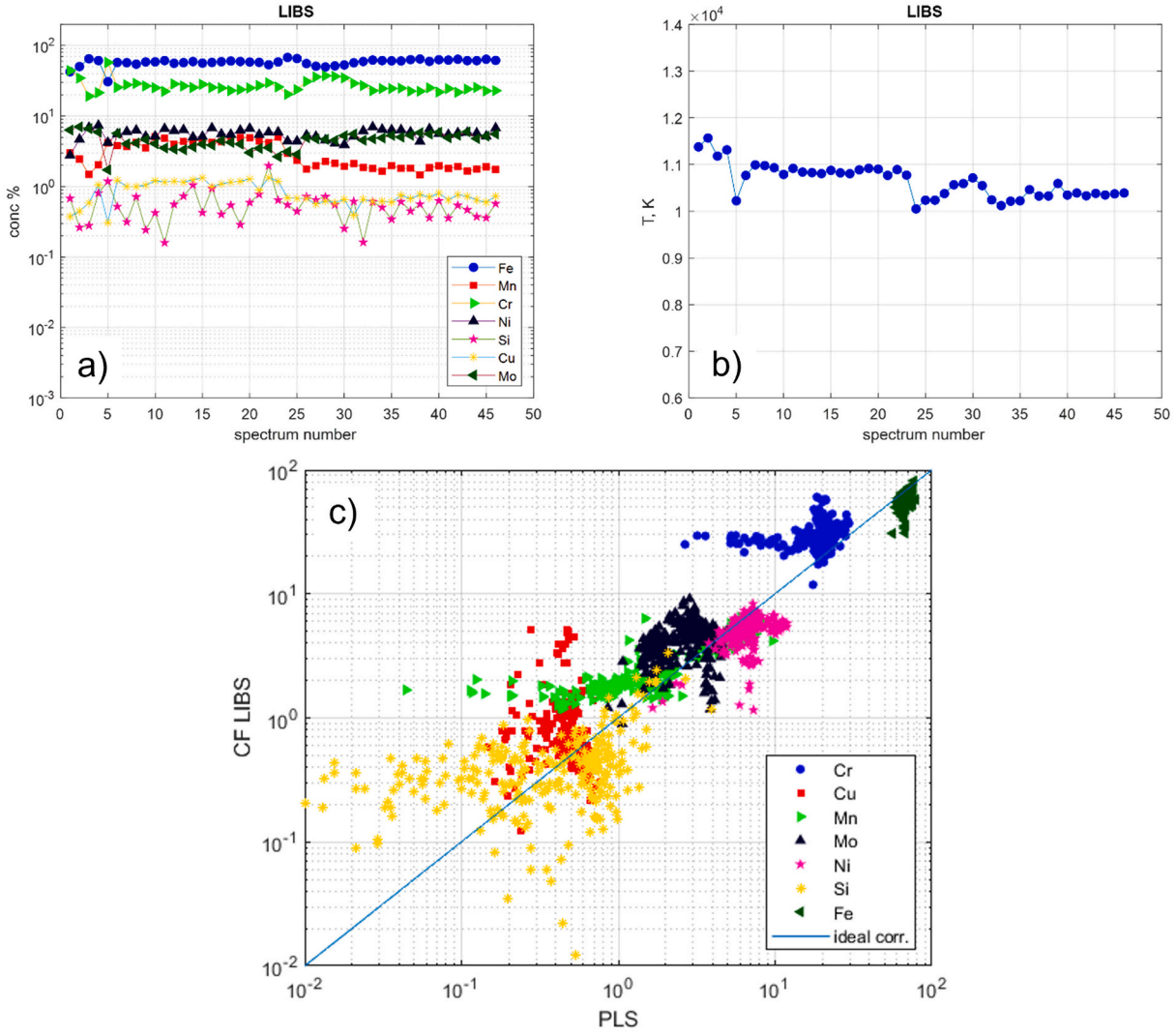

Fig. 5. (a)Variation of element concentrations during GTAW welding, evaluated by CF-LIBS. (b) plasma temperature on a shot-to-shot basis for Ni 6 h sample during GTAW welding. (c) Correlation plot CF LIBS vs PLS-analysis.

plasma. In addition, in Fig. 5 (b) shows the change in electron temperature (T_e) during the welding process. The variations of T_e can be attributed to the aggregate states and the temperature of the sample. The change in plasma T_e can be explained by a change in the aggregate state and temperature of the sample surface. T_e appears to be affected by the temperature-dependent heat capacity and laser ablation rate. A comparison of the two methods shows an agreement within 50%. The correlation of individual concentrations found by the two methods is illustrated by the correlation graph in Fig. 5 (c). Even though the correlation is not perfect, it is sufficient for the task at hand. The CF-LIBS analysis shows a systematic positive or negative bias in elemental concentrations compared to the PLS analysis. Cr, Cu, and Mo concentrations are overestimated by CF-LIBS, while Ni concentrations are underestimated. Mn is detected over a wide range of concentrations in the PLS analysis, while the corresponding range is narrower in the CF analysis. Si exhibits a large scatter, symmetrical to the ideal correlation line in Fig. 5 (c). This means that concentrations below 0.1 wt% cannot be reliably determined by the CF LIBS approach. The large scatter is also due to the fact that the CF-LIBS method uses only one Si line to construct the SBP.

The results of the CF-LIBS are consistent with the analyses of the weld microstructure (Chapter 3.1). The evaporation of alloying elements during TIG welding leads to a change in the microstructure and negatively influences the mechanical properties of the material [22,40]. With the help of CF-LIBS, it was possible to observe in situ how the Mn concentration increases during welding. Since Mn is a strong austenite stabilizer, ferritization of the material occurs, which is clearly visible in Fig. 2. CF-LIBS offers a reliable analysis method for the control and prevention of various weld seam irregularities. To observe the evaporation of various alloying elements and correlate it with the post-weld microstructure, semi-quantitative chemical analysis is likely to be sufficient. This can be justified on the basis of Fig. 5 (a). This would significantly simplify the procedure for analyzing the in situ measurement.

4. Conclusion

The weld microstructure of duplex steels can be controlled by using filler metals coated with either austenite or ferrite stabilizing elements, which changes the respective volume fraction of austenite and ferrite in the weld. This has a significant impact on the physical properties of the resulting part. In this work, the CF-LIBS method is proposed to control the chemical composition of the weld during welding. The results of the CF-LIBS analysis are compared with the results of the calibration-based PLS analysis, and a satisfactory correlation is found. Specifically, Mn evaporation during GTAW welding, which was already identified in previous publications using PLS analysis, is now also confirmed using CF-LIBS. The risk of evaporation of alloying elements during welding is high and must be prevented to ensure the integrity of the welded joints. Thus, the CF-LIBS method offers a significant advantage: the concentrations of key alloying elements that prevent the formation of weld defects can be quickly measured on site without a lengthy calibration procedure. In future work, the information obtained from CF-LIBS analysis will allow direct monitoring of the welding process. In this way, efficient welding processes can be carried out, and hazards that could otherwise only be checked by ex situ methods can be detected directly during the process.

CRediT authorship contribution statement

Lukas Quackatz: Conceptualization, Formal analysis, Investigation, Methodology, Writing – original draft. **Igor Gornushkin:** Data curation, Formal analysis, Software, Writing – review & editing. **Axel Griesche:** Project administration, Supervision, Writing – review & editing. **Thomas Kannengiesser:** Funding acquisition, Supervision, Writing – review & editing. **Kai Treutler:** Investigation, Methodology. **Volker Wesling:** Investigation, Methodology.

Declaration of competing interest

The authors declare that they have no known competing financial interests or personal relationships that could have appeared to influence the work reported in this paper.

Data availability

Data will be made available on request.

Acknowledgements

This work was funded by the Deutsche Forschungsgemeinschaft (DFG, German Research Foundation) – 442001176.

References

[1] Leif. Welding Duplex Stainless Steels — A Review Of Current Recommendations, Welding in the World 56 (5) (2012) 65–76, https://doi.org/10.1007/BF03321351. Yamada, K.; Osuki, T.; Ogawa, K.; Holmes, B.; Sotoudeh, K.; dong, H. Effects of Mo and cu contents on sigma phase precipitation in 25Cr-5Ni-Mo-cu-1Mn-0.18 N duplex stainless steel. ISIJ Int. 2023, 63 (1), 143–149.
[2] M. Knyazeva, M. Pohl, Duplex steels: part I: genesis, formation, Structure, Metallogr. Microstruc. 2 (2) (2013) 113–121, https://doi.org/10.1007/s13632-013-0066-8.
[3] E.M. Westin, Hot cracking in duplex stainless steel weldments — a review, Weldi. World (2022), https://doi.org/10.1007/s40194-022-01310-8.
[4] E.M. Westin, A. Putz, A. Maderthoner, J. Pilhagen, Solidification cracking in duplex stainless steel flux-cored arc welds part 1—cracking in 30-mm-thick material welded under high restraint, Weldi. World (2022), https://doi.org/10.1007/s40194-022-01370-w.
[5] 17781, I. Petroleum, Petrochemical and Natural Gas Industries–Test Methods for Quality Control of Microstructure of Ferritic/Austenitic (Duplex) Stainless Steels. Beuth Berlin, 2017.
[6] I. Varol, J.C. Lippold, W. Baeslack, Welding of duplex stainless steels, in: Key Engineering Materials 69, Trans Tech Publ, 1992, pp. 217–252.
[7] J. Yang, Q. Wang, Z. Wei, K. Guan, Weld failure analysis of 2205 duplex stainless steel nozzle, Case Stud. Eng. Failure Analy. 2 (2) (2014) 69–75, https://doi.org/10.1016/j.csefa.2014.05.001.
[8] A.K. Maurya, C. Pandey, R. Chhibber, Effect of filler metal composition on microstructural and mechanical characterization of dissimilar welded joint of nitronic steel and super duplex stainless steel, Arch. Civil Mechan. Eng. 22 (2) (2022) 90, https://doi.org/10.1007/s43452-022-00413-9.
[9] B. Wittig, M. Zinke, S. Jüttner, Influence of arc energy and filler metal composition on the microstructure in wire arc additive manufacturing of duplex stainless steels, Weldi. World (2020), https://doi.org/10.1007/s40194-020-00995-z.
[10] R. Noll, Laser-Induced Breakdown Spectroscopy Fundamentals and Applications, Springer, 2012.
[11] V. Sturm, H.-U. Schmitz, T. Reuter, R. Fleige, R. Noll, Fast vacuum slag analysis in a steel works by laser-induced breakdown spectroscopy, Spectrochim. Acta B At. Spectrosc. 63 (10) (2008) 1167–1170.
[12] M.A. Sharaf, D.L. Illman, B.R. Kowalski, Chemometrics, John Wiley & Sons, 1986.
[13] E. Tognoni, G. Cristoforetti, S. Legnaioli, V. Palleschi, Calibration-free laser-induced breakdown spectroscopy: state of the art, Spectrochim. Acta B At. Spectrosc. 65 (1) (2010) 1–14, https://doi.org/10.1016/j.sab.2009.11.006.
[14] A.J.R. Bauer, S.G. Buckley, Novel applications of laser-induced breakdown spectroscopy, Appl. Spectrosc. 71 (4) (2017) 553–566.
[15] O. Forni, M. Gaft, M.J. Toplis, S.M. Clegg, S. Maurice, R.C. Wiens, N. Mangold, O. Gasnault, V. Sautter, S. Le Mouélic, First detection of fluorine on Mars: implications for Gale Crater's geochemistry, Geophys. Res. Lett. 42 (4) (2015) 1020–1028.
[16] A. Ciucci, M. Corsi, V. Palleschi, S. Rastelli, A. Salvetti, E. Tognoni, New procedure for quantitative elemental analysis by laser-induced plasma spectroscopy, Appl. Spectrosc. 53 (8) (1999) 960–964.
[17] B. Praher, V. Palleschi, R. Viskup, J. Heitz, J. Pedarnig, Calibration free laser-induced breakdown spectroscopy of oxide materials, Spectrochim. Acta B At. Spectrosc. 65 (8) (2010) 671–679.
[18] J.D. Pedarnig, P. Kolmhofer, N. Huber, B. Praher, J. Heitz, R. Rössler, Element analysis of complex materials by calibration-free laser-induced breakdown spectroscopy, Appl. Phys. A 112 (2013) 105–111.
[19] EWM, EWM Welding Dictionary, 2009.
[20] H.-Y. Tseng, Welding parameters optimization for economic design using neural approximation and genetic algorithm, Int. J. Adv. Manuf. Technol. 27 (9–10) (2006) 897–901.
[21] P.A.A. Khan, T. Debroy, Alloying element vaporization and weld Pool temperature during laser-welding of Aisi 202 stainless-steel, Metall. Trans. B 15 (4) (1984) 641–644, https://doi.org/10.1007/Bf02657284.
[22] M.M. Collur, A. Paul, T. Debroy, Mechanism of alloying element vaporization during laser-welding, Metall. Trans. B 18 (4) (1987) 733–740, https://doi.org/10.1007/Bf02672891.

[23] A. Blockbolten, T.W. Eagar, Metal vaporization from weld pools, Metallur. Trans. B-Process Metallur. 15 (3) (1984) 461–469.
[24] J. Mirapeix, A. Cobo, O.M. Conde, C. Jaúregui, J.M. López-Higuera, Robust technique for spectroscopic plasma analysis with application in real-time arc welding quality monitoring, OPTICE 45 (8) (2006), https://doi.org/10.1117/1.2336416, 083002–083002-083005.
[25] J.J. Valdiande, M. Martínez-Minchero, A. Cobo, J.M. Lopez-Higuera, J. Mirapeix, On-line monitoring and defect detection of arc-welding via plasma optical spectroscopy and LIBS, Spectrochim. Acta B At. Spectrosc. 194 (2022) 106474, https://doi.org/10.1016/j.sab.2022.106474.
[26] V.N. Lednev, P.A. Sdvizhenskii, R.D. Asyutin, R.S. Tretyakov, M.Y. Grishin, A. Y. Stavertiy, S.M. Pershin, In situ multi-elemental analysis by laser induced breakdown spectroscopy in additive manufacturing, Addit. Manuf. 25 (2019) 64–70, https://doi.org/10.1016/j.addma.2018.10.043. Lednev, V. N.; Sdvizhenskii, P. A.; Grishin, M. Y.; Stavertiy, A. Y.; Tretyakov, R. S.; Asyutin, R. D.; Pershin, S. M. Laser Welding Spot Diagnostics by Laser-Induced Breakdown Spectrometry. Physics of Wave Phenomena 2021, 29 (3), 221-228. DOI: 10.3103/S1541308X21030092.
[27] V. Lednev, P. Sdvizhenskii, A.Y. Stavertiy, M.Y. Grishin, R. Tretyakov, R. Asyutin, S. Pershin, Online and in situ laser-induced breakdown spectroscopy for laser welding monitoring, Spectrochim. Acta B At. Spectrosc. 175 (2021) 106032.
[28] V.N. Lednev, P.A. Sdvizhenskii, M.Y. Grishin, A.Y. Stavertiy, R.S. Tretyakov, R. D. Asyutin, A.N. Fedorov, S.M. Pershin, In situ laser-induced breakdown spectroscopy measurements during laser welding of superalloy, Appl. Opt. 60 (5) (2021) 1144–1149, https://doi.org/10.1364/AO.411359.
[29] U.A. Taparli, T. Kannengiesser, K. Cieslik, D. Mory, A. Griesche, In situ chemical composition analysis of a tungsten-inert-gas austenitic stainless steel weld measured by laser-induced breakdown spectroscopy, Spectrochim. Acta B At. Spectrosc. (2020) 105826, https://doi.org/10.1016/j.sab.2020.105826.
[30] U.A. Taparli, L. Jacobsen, A. Griesche, K. Michalik, D. Mory, T. Kannengiesser, In situ laser-induced breakdown spectroscopy measurements of chemical compositions in stainless steels during tungsten inert gas welding, Spectrochim. Acta B At. Spectrosc. 139 (2018) 50–56, https://doi.org/10.1016/j.sab.2017.11.012.
[31] L. Quackatz, A. Griesche, T. Kannengiesser, In situ investigation of chemical composition during TIG welding in duplex stainless steels using laser-induced breakdown spectroscopy (LIBS), Force. Mechan. 6 (2022) 100063, https://doi.org/10.1016/j.finmec.2021.100063.
[32] L. Quackatz, A. Griesche, T. Kannengiesser, Spatially resolved EDS, XRF and LIBS measurements of the chemical composition of duplex stainless steel welds: a comparison of methods, Spectrochim. Acta B At. Spectrosc. 193 (2022) 106439, https://doi.org/10.1016/j.sab.2022.106439.
[33] L. Quackatz, A. Griesche, T. Kannengiesser, Rapid solidification during welding of duplex stainless steels – in situ measurement of the chemical concentration by laser-induced breakdown spectroscopy (LIBS), IOP Conf. Series: Materi. Sci. Eng. 1274 (1) (2023) 012018, https://doi.org/10.1088/1757-899X/1274/1/012018.
[34] DIN, Nichtrostende Stähle – Teil 1: Verzeichnis der nichtrostenden Stähle; Deutsche Fassung EN 10088–1:2014, 2020.
[35] K. Treutler, Schweißen von Leichtbaurahmenkonstruktionen: funktionale Werkstoffauswahl und Schweißzusatzwerkstoffmodifikation, Dissertation, 2019, Technische Universität Clausthal, Clausthal-Zellerfeld, 2019.
[36] V. Wesling, A. Schram, T. Müller, K. Treutler, Influencing the arc and the mechanical properties of the weld metal in GMA-welding processes by additive elements on the wire electrode surface, IOP Conf. Series: Materi. Sci. Eng. 118 (1) (2016) 012006, https://doi.org/10.1088/1757-899X/118/1/012006.
[37] F. Chen, W. Lu, Y. Chu, D. Zhang, C. Guo, Z. Zhao, Q. Zeng, J. Li, L. Guo, High accuracy analysis of fiber-optic laser-induced breakdown spectroscopy by using multivariate regression analytical methods, Spectrochim. Acta B At. Spectrosc. 106160 (2021), https://doi.org/10.1016/j.sab.2021.106160.
[38] C.R. Ytsma, M.D. Dyar, Effects of univariate and multivariate regression on the accuracy of hydrogen quantification with laser-induced breakdown spectroscopy, Spectrochim. Acta B 139 (2018) 27–37, https://doi.org/10.1016/j.sab.2017.11.010.
[39] I.B. Gornushkin, T. Völker, A.Y. Kazakov, Extension and investigation by numerical simulations of algorithm for calibration-free laser induced breakdown spectroscopy, Spectrochim. Acta B At. Spectrosc. 147 (2018) 149–163.
[40] H. Park, M. Trautmann, K. Tanaka, M. Tanaka, A.B. Murphy, A computational model of gas tungsten arc welding of stainless steel: the importance of considering the different metal vapours simultaneously, J. Phys. D. Appl. Phys. 51 (39) (2018) 395202, https://doi.org/10.1088/1361-6463/aad74c.